PAPER

Analysis of the deviations from the similarity between JET and ITER ion cyclotron resonance heating

IOP Publishing | International Atomic Energy Agency Nuclear Fusion

Nucl. Fusion **59** (2019) 126006 (7pp) https://doi.org/10.1088/1741-4326/ab3eae

Analysis of the deviations from the similarity between JET and ITER ion cyclotron resonance heating

Jungpyo Lee[1,2], **Roberto Bilato**[3] and **Erwin F. Jaeger**[4]

[1] Hanyang University, Nuclear Engineering Department, Seoul, Korea, Republic of
[2] MIT Plasma Science and Fusion Center, Cambridge, MA, United States of America
[3] Max Planck Institute for Plasma Physics, Garching, Germany
[4] XCEL Engineering, Oak Ridge, TN, United States of America

E-mail: jungpyo@hanyang.ac.kr

Received 23 March 2019, revised 8 July 2019
Accepted for publication 27 August 2019
Published 18 September 2019

Abstract

To predict the performances of ion-cyclotron resonance heating in ITER based on the existing JET experimental results, it is important to know the impact of the deviations from the exact similarity relations between these two tokamaks. For this aim, in this paper we identify three global scaling parameters depending on the main plasma/wave quantities, such as confining magnetic fields, major radius, plasma density and temperature, wave frequency, toroidal mode number, and absorbed wave power to describe the important difference between JET and ITER. By introducing three new scaling parameters to capture the Doppler effect, the plasma beta, and the fast ion kinetic effect, ITER will be expected to have a lower optimized minority concentration, a higher fraction of electron damping, a lower ion effective temperature. When the deviation from the exact scaling relations is not significant, the new scaling parameters represent sufficiently the linear change of the predicted results of ITER from the reference results of JET. Some inter-dependent nonlinear effects between the new scaling parameters are also examined.

Keywords: ion cyclotron resonance heating, similarity, wave physics, tokamak, kinetic effect, wave power partition

(Some figures may appear in colour only in the online journal)

Introduction

Experiments on propagation and absorption of radio-frequency (RF) waves in the ion cyclotron range of frequency (ICRF) done in present fusion devices are essential to design ICRF-heating systems and ICRF scenarios for reactor-size devices [1–6]. Indeed, several JET experiments [7–12] have been designed to address ICRF physics specifically for ITER [13–15]. Part of these experiments have been done to investigate the minority ion fundamental heating in (^{3}He)H, (^{3}He)D, (^{3}He)D–T plasmas, and the first harmonic heating in (H)D plasmas. Here, the species in parenthesis is the RF-heated minority species. The similar propagation and damping of ICRF waves between two tokamaks were expected when some key-parameters such as the wave frequency and the toroidal mode number of antenna are matched.

The conditions of an exact (self) similarity between two different ICRF devices was investigated in our previous study [16] by finding the constraints of an exact equivalence by rigidly rescaling (1) Maxwell's equations for the wave propagation and absorption, (2) the Grad–Shafranov equation for the magnetic equilibrium, and (3) the Fokker–Planck equation for the kinetic impact of ICRF heating on the collisional-time scale. The scaling conditions of the exact similarity are

$$\eta_\omega = \eta_B,\ \eta_n = \eta_B^2,\ \eta_R = \eta_B^{-1},\ \eta_P = \eta_B,\ \eta_{n_\phi} = \eta_{I_p} = \eta_T = 1, \quad (1)$$

where the scaling factor η_x is introduced for $\bar{x} = \eta_x x$, and $\bar{x}$ is the scaled quantity of x. The quantity x can be the tokamak

size R, the background magnetic fields B, the plasma current I_p, the plasma density n, the temperature T, the wave frequency ω, the toroidal mode number n_ϕ, and the total absorbed wave power P. In this analysis, it is implicitly assumed that the relative geometries (aspect ratio) are not changed in the scaling, as it is indeed the case that those of present and future devices are roughly similar. When the scaling relations are satisfied with the same plasma composition, the ICRF waves in plasmas of two tokamaks are exactly equivalent, as proven by numerical simulations [16]. However, the scaling for the exact similarity in real experiments is hardly attainable due to physical and practical reasons. The constraint on the temperature $\eta_T = 1$ is difficult to achieve due to anomalous transport and the constraint on the size $\eta_R = \eta_B^{-1}$ is also questionable in the reactor-size device.

Table 1 summarizes the different parameters of ICRF systems between JET and ITER for the (^{3}He)D–T discharge. The fundamental similarity of the scaling between JET and ITER is obtained by $\eta_\omega = \eta_B$ and $\eta_{n_\phi} = 1$. We always keep the necessary constraints $\eta_\omega = \eta_B$ and the same relative geometry in the simulations of this study. However, for ITER the scaling of the machine size and the magnetic fields are fixed as $\eta_R \simeq 2$ and $\eta_B \simeq 1.4$, and the estimated temperature and density profile of the ICRF scenarios have $\eta_n \simeq 2.6$, and $\eta_T \simeq 2$ compared to the JET D–T discharge 41725 [12]. Thus, the exact similarity of the ICRF heating scenarios between present devices and reactor-size plasmas cannot be achieved, and part of the similarity must be sacrificed. However, this fact does not prevent the acquisition of important information for reactor-size plasmas in present devices when it is known which part of the similarity is missing. The fact that $\eta_T > 1$ can be partially compensated in the Doppler shift and electron Landau damping by tailoring η_{n_ϕ} with the antenna design and its operation. Analogous compensation is difficult for finite Larmor radius (FLR) effects, which are important in the case of IC harmonic heating. It is important to investigate the impact of these differences on the deviations from the exact similarity.

In this paper, the similarity degree between JET experiments and ICRF scenarios on ITER is studied systematically by means of three scaling parameters D_1, D_2 and D_3, identified by (1) optimizing the concentration of the ICRF-heated minority species to have maximum direct RF ion heating, (2) evaluating the direct RF power partition to each species, and (3) finding effective temperatures of the heated species for the effects of fast ions produced by ICRF heating. These simple scaling parameters fetch some of the salient aspects of the ICRF wave propagation and absorption in the plasma, but they cannot capture nonlinear physics phenomena such as the differences related to the plasma–wall interactions as consequence of different wall materials. Indeed, the ITER wall will be different from the carbon wall of the JET discharge we are considering as the reference here. However, it is out of the scope of this work to account also of the impact of plasma–wall interaction as consequence of ICRF heating on the plasma parameters. The plasma parameters are pre-defined in this analysis.

Table 1. A comparison between JET and ITER ICRF systems.

	JET (^{3}He) D–T shot 42725 [12]	ITER (^{3}He) D–T [13, 14]
Wave frequency (MHz)	37	53.5 ($\eta_\omega = 1.44$)
Major radius (m)	3	6 ($\eta_R = 2.0$)
Magnetic fields (T)	3.7	5.35 ($\eta_B = 1.44$)
Plasma current (MA)	3.3	15 ($\eta_{I_p} = 4.54$)
Core density (10^{20} m^{-3})	0.38	1.0 ($\eta_n = 2.63$)
Core temperature (KeV)	12	24 ($\eta_T = 2.0$)
Toroidal mode	27	27 ($\eta_{n_\phi} = 1.0$)
RF power (MW)	5	20 ($\eta_P = 4.0$)

Optimized minority concentration

The wave damping mechanisms in the (^{3}He) D–T plasma can be explained by two characteristic lengths [1–6]. When the fundamental cyclotron resonance with the minority species occurs at the plasma center with $\omega_{cm} > \omega_{cM}$, the ion–ion cut-off layer ($n_\parallel^2 = \mathcal{L}$) exists on the high-field side, and it is located between the cyclotron resonance at the center and the ion-hybrid resonance layer ($n_\parallel^2 = \mathcal{S}$) on the high-field side, where $n_\parallel$ is the parallel refractive index, $\mathcal{L}$ and $\mathcal{S}$ are the Stix dielectric tensor components [5] and ω_{cm} and ω_{cM} are the cyclotron frequencies ($\omega_c = ZqB/m$) of minority species and majority species, respectively. For the wave launched from the low field side, there is an evanescent region between the cut-off layer and the ion-hybrid resonance layer, and the distance between the layers (evanescence distance) is characterized by the effective evanescence length, $\delta \simeq (n_m/n)R$ [6]. Here, n_m/n is the fraction of the minority species density to the total density. The second characteristic length is the width of the resonance by Doppler effects, $\Delta \simeq n_\parallel(v_{ti}/c)R$, where v_{ti} is ion thermal velocity and c is the speed of light.

Although there is an additional damping mechanism in the (^{3}He)D–T plasmas by the first harmonic damping of tritium, which occurs at the same location of the fundamental damping of ^{3}He, the comparison between Δ and δ is still effective to capture the nature of the dominant damping mechanism. When $\Delta > \delta$, the minority damping becomes dominant over the mode conversion into ion-Bernstein wave (IBW), which are eventually absorbed by electrons. This usually occurs at low to medium minority concentration, depending on the plasma composition ($n_m/n < 0.05$). The optimized minority fraction (n_m/n) for the maximum minority damping is determined by the ratio of the two lengths.

The scaling of the length ratio is determined by

$$\overline{(\Delta/\delta)} \simeq D_1(\Delta/\delta), \tag{2}$$

where the scaling parameter D_1 is

$$D_1 = \frac{\eta_{n_\phi}\sqrt{\eta_T}}{\eta_B\eta_R}. \tag{3}$$

The increase of the ratio Δ/δ with D_1 results in the increase of the optimized concentration due to the larger Doppler effect.

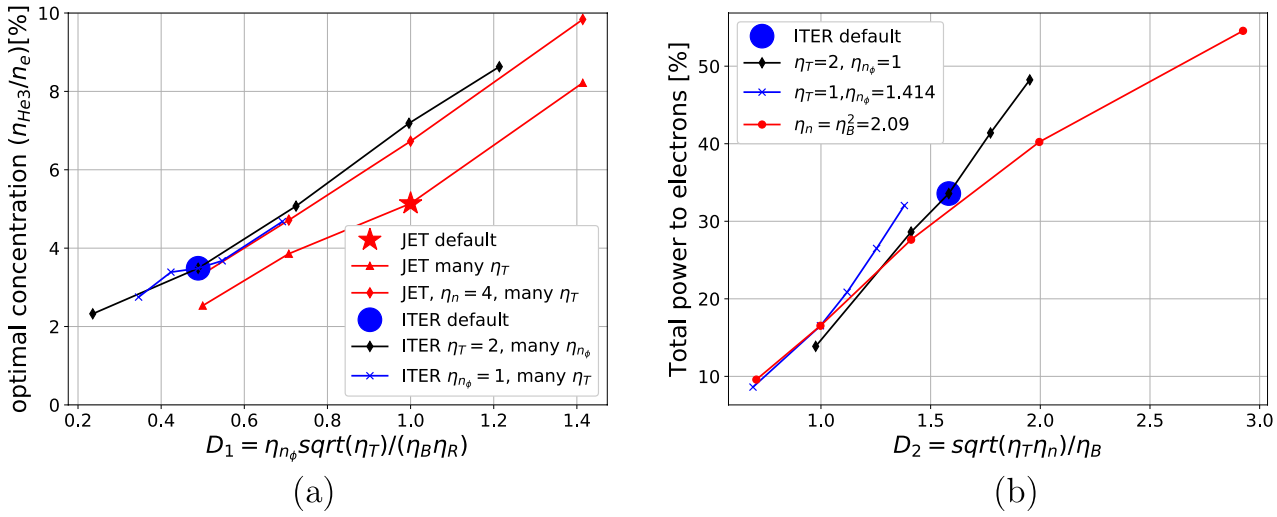

Figure 1. (*a*) The optimized minority fraction for the maximum ion damping in terms of D_1. (*b*) Electron damping percentage in terms of D_2 with the optimized concentration from (*a*) for ITER. For (*a*), the density is fixed by the relation of equation (1) $\eta_n = \eta_B^2$ for ITER. For (*b*), the black and blue lines use the different densities at the same $D_1 = 0.49$ for ITER, and the red line changes the temperature with the fixed density.

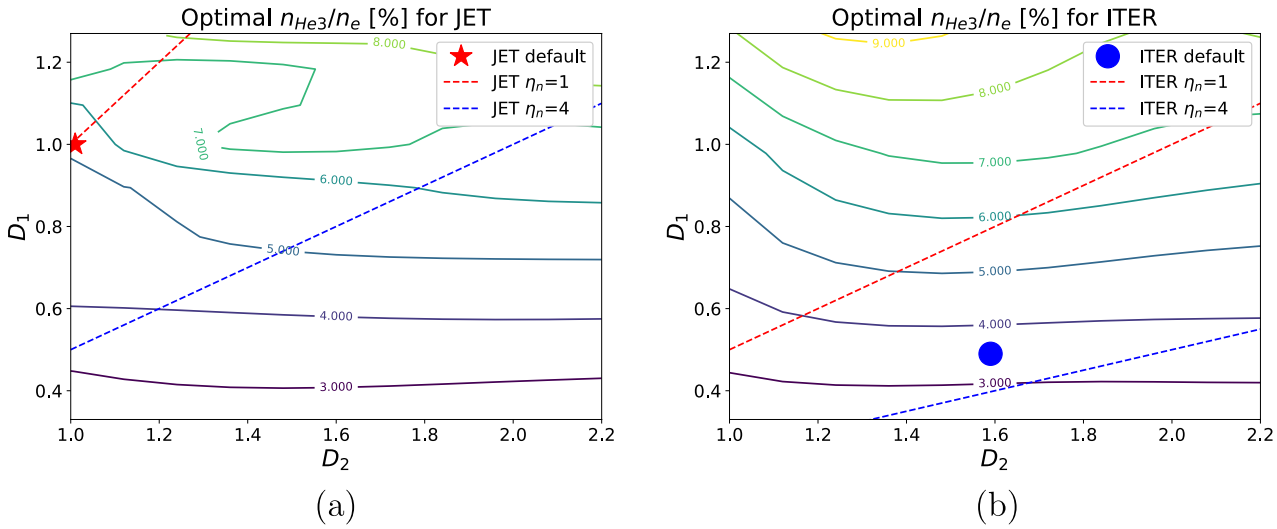

Figure 2. Contour plot of the optimal minority fraction in terms of D_1 and D_2 for (*a*) JET and (*b*) ITER. D_1 is adjusted by the different temperature η_T, and D_2 is adjusted by the different density η_n, where $\eta_{n_\phi} = 1$.

Figure 1(*a*) shows the optimized minority fraction to the electron density n_{He3}/n_e for the maximum ion damping percentage by the simulations of the full wave code, TORIC [17]. The simulation parameters of the default cases for JET and ITER are selected as in the table 1, giving $D_1 = 0.49$ for ITER compared to the JET reference ($D_1 = 1$). The optimal concentration is likely proportional to the scaling parameter D_1, regardless of different set of temperature (η_T), toroidal mode number (η_{n_ϕ}), magnetic fields (η_B) and machine size (η_R) scalings. The optimal concentration in the JET default density cases is somewhat smaller than that of ITER for the same D_1 in figure 1(*a*), which will be clarified wtih figure 2.

Power partition

The maximum percentage of the minority ion damping at the optimal minority fraction changes depending on the plasma density and temperatures. As shown in figure 1(*b*), the damping to ^{3}He species decreases and electron damping increases, when the plasma beta increases. Here, the plasma beta is scaled by

$$\overline{\beta} = D_2^2 \beta, \tag{4}$$

where the new scaling parameter D_2 is

$$D_2 = \frac{\sqrt{\eta_T \eta_n}}{\eta_B}. \tag{5}$$

Figure 1(*b*) shows the similar increase of the electron Landau damping by D_2 for the different temperature and density. The increased electron Landau damping compared to the ion cyclotron damping can be explained in the following reasons. As shown in [2], the polarization of the electric field becomes more inefficient for the cyclotron damping as the increase of the density. Additionally, the amount of the

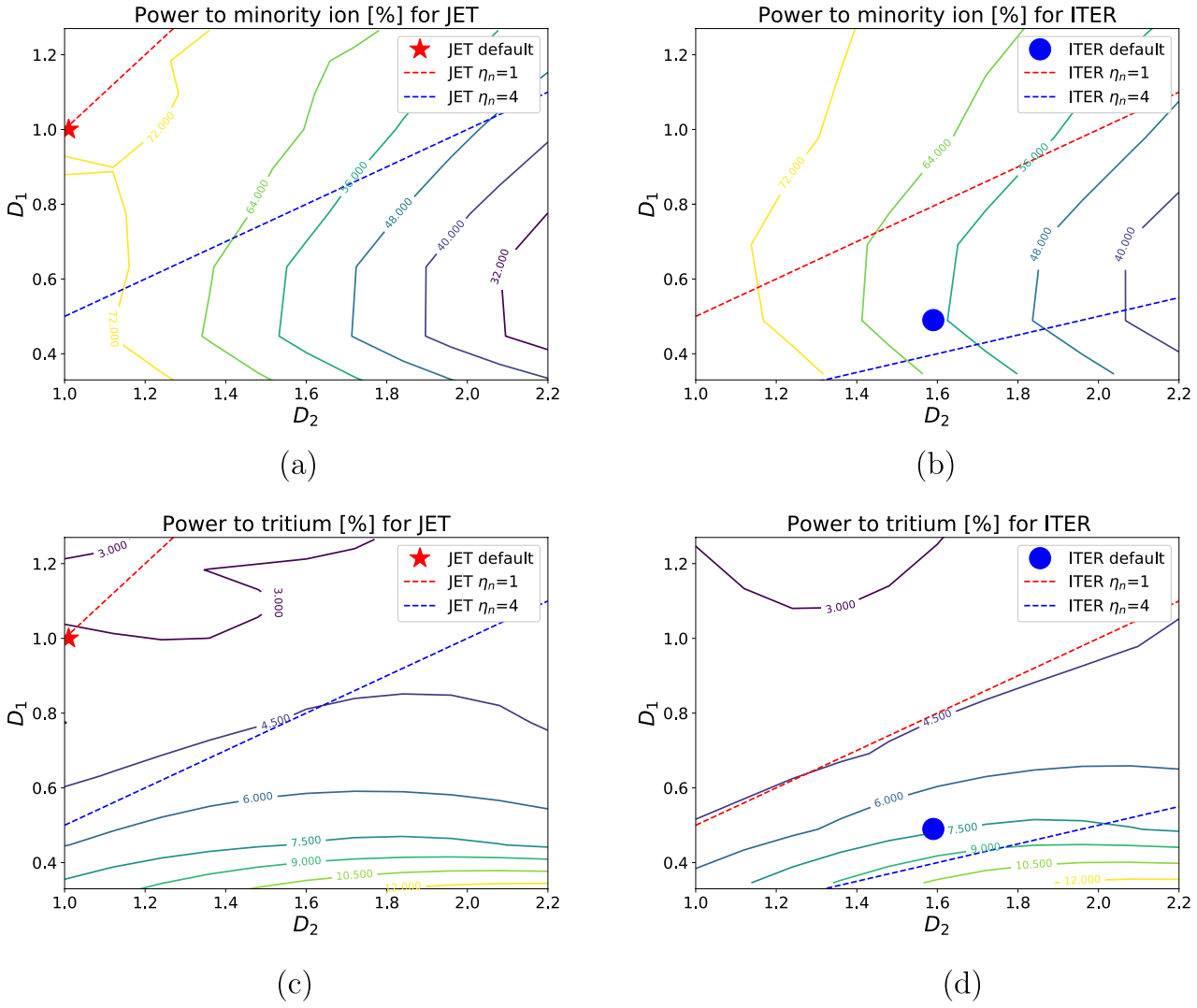

Figure 3. Contour plot of the power partition percentage in terms of D_1 and D_2 at the optimal minority fraction for (a) ^{3}He $n = 1$ damping of JET, (b) ^{3}He $n = 1$ damping of ITER, (c) tritium $n = 2$ damping of JET, and (d) tritium $n = 2$ damping of ITER. D_1 is adjusted by the different temperature η_T, and D_2 is adjusted by the different density η_n, where $\eta_{n_\phi} = 1$.

reflection from the cut-off layer $n_\parallel^2 = \mathcal{L}$ increases [5], and it result in more possibilities of the electron Landau damping on the multi-path of the fast wave. The perpendicular wave vector of the fast wave branch increases by density,

$$n_\perp = \frac{k_{\perp,\mathrm{fast}} c}{\omega} \simeq \frac{\omega_{pM}}{\omega_{cM}} \propto \sqrt{n} \tag{6}$$

and the reflection coefficient ($\mathcal{R}$) of the fast wave increases by $\mathcal{R} = (1 - \mathrm{e}^{-\alpha})^2$ where $\alpha \propto k_{\perp,\mathrm{fast}}\delta$ [6].

The electron damping increase by D_2 can be applicable to the limited cases (e.g. our JET and ITER reference cases), when the ion damping is dominant over the electron damping and the wave has the multi-path between two cut-off layers in the core and in the edge. For a single-pass damping or the electron dominated damping, it could be more important to consider the geometrical effects of the different size tokamaks globally.

Although the optimal concentration and the power decomposition are dominantly determined by D_1 and D_2, respectively, as shown in figures1(a) and (b), they are not the only important independent variables. The contour plots in figure 2 show that the change of D_2 by different density can change the optimal concentration, if D_1 is sufficiently large (e.g. $D_1 > 0.6$). It is worth noting that the contour patterns and values between JET in figure 2(a) and ITER in figure 2(b) are similar in the low D_1 range, while they are different in the large D_1 range. The dashed lines are denoted for the reference of the correlation between D_1 and D_2 with the fixed density, magnetic field, and machine size, giving $D_1 = D_2(\eta_{n_\phi}/\sqrt{\eta_n}\eta_R)$ but the varying temperature. The changes of the optimal concentration along the reference lines $\eta_n = 1$ and $\eta_n = 4$ explain the different graphs of figure 1(a) for JET, which is mostly by the complicated pattern of figure 2(a) due to the dependence of plasma beta on the IBW coupling.

The contour plots in figure 3 show the effects of D_1 as well as D_2 on the power decomposition at the optimal minority fraction. Because the electron Landau damping more likely occurs when the wave interacts with thermal electrons for the larger parallel refractive index, the electron damping generally increases and the ion damping decreases by D_1 due to

the Doppler effect scaling $\overline{k_\parallel v_{ti}/\omega} \simeq D_1(k_\parallel v_{ti}/\omega)$. Thus, the effect of the temperature increase on the electron Landau damping and the main dependence on the machine size for the multi-path case are well captured in the parameter D_1.

Figure 3 also shows the notably different characteristics between ^{3}He fundamental ($n = 1$) damping in (a) and (b) and tritium first harmonic ($n = 2$) damping in (c) and (d). The tritium $n = 2$ damping increases in the direction of the increase of the density alone (the dashed lines) by the relation between D_1 and D_2. The density dependency of $n = 2$ damping can be understood by the finite Larmor radius effect in equation (6). It is also worth noting that D_1 and D_2 show the similar patterns between JET and ITER in figure 3, so D_1 and D_2 are the important scaling parameters for such physics between different tokamaks.

Kinetic effects

The scaling parameter D_3 represents the degree of the change in the distribution function of the ICRF-heated ion species, and it is closely related to the effective temperature ($T_{\rm eff}$), which was studied in [18]. For a simple explanation using the bounce averaged Fokker–Planck equation, the increase of the temperature by the low or moderate power density can be calculated in the linearization of the distribution function by the perturbed distribution f_1 from the equilibrium distribution function f_0. If one assumes the quasilinear diffusion $\mathbf{D}$ is mostly determined by f_0 and the collision term is determined by f_1 because of $C(f_0) = 0$, it results in the scaling of the Fokker–Planck equation, $D_3\overline{(\nabla_v \cdot \mathbf{D} \cdot \nabla_v f_0)} = \overline{C(f_1)}$, where

$$D_3 = \frac{\eta_P \eta_T^{1/2}}{\eta_n^2 \eta_R^3} = \eta_P \frac{D_1^5}{D_2^4} \frac{\eta_B \eta_R^2}{\eta_{n_\phi}^5}. \tag{7}$$

One can show that $D_1 = 1$, $D_2 = 1$, and $D_3 = 1$ in the exact scaling of equation (1).

Because D_3 determines the scaling of f_1, one can approximate the scaling of the temperature increase due to the RF waves in the linear regime by

$$\overline{\left(\frac{T_{\rm RF}}{T_0} - 1\right)} \simeq D_3 \left(\frac{T_{\rm RF}}{T_0} - 1\right), \tag{8}$$

where $T_{\rm RF}$ and T_0 are the temperature after RF wave injection and before the injection, respectively. D_3 could be useful to describe some nonlinear physics associated with the RF wave power density such as the synergy effect between the neutral beam injection and ICRF injection, although the nonlinear physics is beyond the scope of the paper. In principle, ITER would have a smaller synergy effect than JET because of the low power densities ($D_3 < 1$).

The relation of equation (8) holds well in the range of ITER parameters (small $|f_1/f_0|$) either for fundamental cyclotron damping or for the first harmonic damping. In this paper, we examine the first harmonic cyclotron damping to see the FLR kinetic effect, and simulate the JET discharge 58734 parameters of the first harmonic hydrogen heating in (H)D plasmas [7], which has $P_{\rm abs} = 5$ MW, $n_{e0} = 4 \times 10^{19}$ m^{-3}, $n_H/n_e = 3\%$, $n_\phi = 27$, $T_{e0} = 3$ KeV, $B_0 = 1.65$ T, $I_p = 1.65$ MA, $\omega = 2\omega_H = 51$ MHz, as a JET default case. Compared to the JET default case, the ITER parameters are selected as the scaling by $\eta_B = 1.5$, $\eta_R = 2$, $\eta_T = 4$ for the (H)D plasmas.

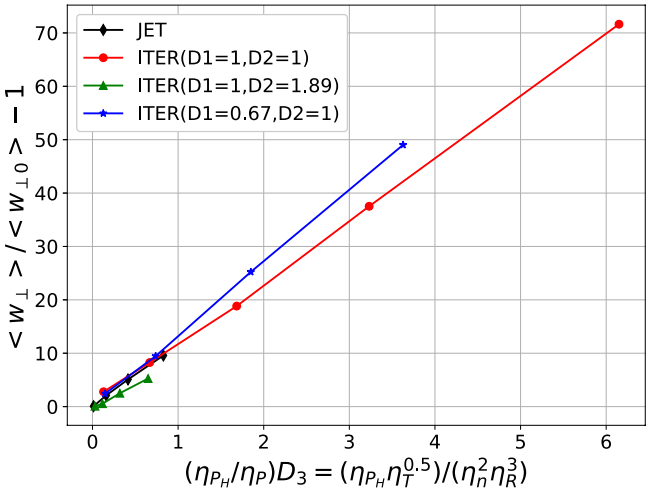

Figure 4. Increase of the volume averaged perpendicular temperature $\langle w_\perp/w_\perp(t=0)\rangle - 1$ in terms of $(\eta_{P_H}/\eta_P)D_3$ due to the first harmonic ICRF damping using the self-consistent AORSA-CQL3D simulations. For the curves of $D_1 = 1$ and $D_2 = 1$, $\eta_{n_\phi} = 1.5$ and $\eta_n = 0.5625$ are used. For $D_1 = 0.67$, $\eta_{n_\phi} = 1.0$ is used. For $D_2 = 1.89$, $\eta_n = 2$ is used.

Figure 4 shows the increase of the perpendicular temperature $(w_\perp - w_\perp(t=0))/w_\perp(t=0)$ due to the cyclotron damping using the self-consistent distribution evolution in the coupled Maxwell's equation solver (AORSA) [19] and Fokker–Planck equation solver (CQL3D) [20]. Here, $w_\perp = \int {\rm d}^3 v (m v_\perp^2/2) f$ represents the perpendicular energy. For the fixed D_1 and D_2, the wave power is adjusted to simulate each value of D_3 in the figure.

Figure 4 indicates that the increase of the volume averaged temperature is likely proportional to the scaling parameter D_3 even for the first harmonic damping. However, as indicated in the JET experiments [7], the increase of the temperature due to the first harmonic damping of hydrogen species is not well consistent with the effective temperature estimation in [18], if other parameters (e.g. D_1 and D_2) change. For the different D_1 or the different D_2, the slopes are different from that of $D_1 = 1$ and $D_2 = 1$ in figure 4. The different D_1 makes the different resonance condition, and the different D_2 results in the change of $k_\perp$, which is significantly connected with the FLR effect for the first harmonic mode. The FLR effect is determined by the Bessel function of the first kind, $J_1(k_\perp \rho_i)$ of the quasilinear diffusion term [21], and the first zero of the function occurs when $k_\perp \rho_i = 3.83$, which corresponds to the perpendicular energy $E^* \simeq 1$ MeV for the JET discharge 58734 [7].

Figure 5 shows the contour plot of the temperature increase due to the first harmonic damping in terms of the different density by D_2 and the different power to hydrogen by $(\eta_{P_H}/\eta_P)D_3$ where η_{P_H}/η_P is the power ratio of the hydrogen first harmonic damping to the total damping. In the contours, the temperature increase is almost proportional to $(\eta_{P_H}/\eta_P)D_3$, while it also varies significantly by D_2. As the density and D_2 increase, the

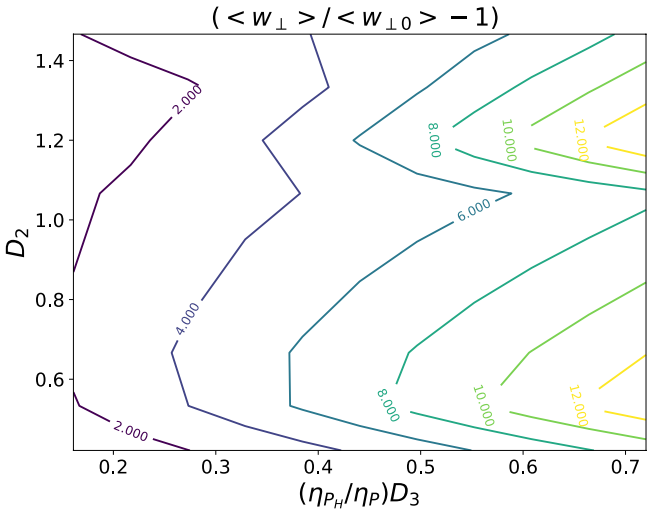

Figure 5. Increase of the volume averaged perpendicular temperature in terms of D_2 and $(\eta_{P_H}/\eta_P)D_3$ with $D_1 = 1$. D_2 is adjusted by the different density η_n, and D_3 is adjusted by the different power η_P.

contribution of the Bessel function $J_1(k_\perp \rho_i)$ to the non-Maxwellian shape changes by equation (9), and its contribution to the perpendicular temperature also changes. The average of the Bessel function argument has the scaling by D_2,

$$\overline{(k_\perp \rho_{ti})^2} \simeq D_2^2 (k_\perp \rho_{ti})^2, \tag{9}$$

where $\rho_{ti} = v_{ti}/\omega_c$ and equation (6) is used. Because the generation of the tail by the quasilinear velocity diffusion cannot be fully represented by the perpendicular temperature [22], the relation between D_2 and the perpendicular temperature increase is complicated.

Conclusions

In this paper, we define three scaling parameters, D_1, D_2 and D_3 which represent physically the scaling of the Doppler effect, the plasma beta (or the FLR effect) and the effective temperature, respectively. We use these parameters to explore the simulation results of a system (i.e. ITER ICRF), in which its scaling relations to the reference system (i.e. JET ICRF) deviate from the exact similarity condition in equation (1), in the direction of the single parameter change in the phase space or multi-parameter changes around the linear regime from the reference point. The effects of the single scaling parameters can be summarized as followings: As the increase of D_1, the optimal concentration of the minority species for the maximum ion damping increases almost proportionally. As the increase of D_2, the minority ion damping at the optimal concentration decreases and the electron damping increases significantly. As the increase of D_3, the volume averaged temperature of the resonant ion species increases almost proportionally. The inter-dependent nonlinear effects of the multi-parameter are shown in the contours of figures 2, 3 and 5.

For the ITER design parameters in table 1, the scaling parameters have $D_1 = 0.49$, $D_2 = 1.59$ for the (^{3}He)D–T minority fundamental damping scenario, and $D_3 = 0.055$ for (H)D first harmonic damping scenario. As a result, the optimal minority concentration of the ^{3}He plasmas fundamental damping is reduced from $n_{\mathrm{He3}}/n_e \simeq 0.05$ of JET to $n_{\mathrm{He3}}/n_e \simeq 0.03$ in ITER [23]. The ion damping at the optimal minority concentration in ITER is reduced by the increase of D_2. Accordingly, the electron damping can be approximately 34% of the total power damping, as shown in other benchmark paper of ITER [14]. Compared to the hydrogen temperature increase due to first harmonic damping in JET, the temperature increase in ITER will be reduced by the factor of $D_3 = 0.055$ approximately.

Although the accurate simulations are required to predict the ITER ICRF heating performance in details, the simple scaling relation rules using the representative 0D parameters D_1, D_2, and D_3 are still beneficial by two reasons. The first reason is that the 0D parameters for ICRF physics can provide the useful interpretative tool for some experimental results and simulation results, as the 0D parameters for transport physics such as $\rho_\star$ and $\nu_\star$ are used to interpret the tendency of the experiments and simulations by representing the local turbulence physics and the collisionality. The second reason is that the simple scaling can be used for the initial design process, which requires checking thousands of design candidates whose parameters vary in multi-dimensional phase space. After finding the desirable area of the design parameter space using the 0D parameters, we can conduct the significantly reduced number of the detailed simulation with the small parameter space area. This initial pre-process of the design can reduce the effort and the cost of the design process significantly.

Acknowledgments

This work was supported by the research fund of Hanyang University (HY-2018). This research used computer resources of MIT and NERSC by the US DoE Contract No. DE-AC02-05CH11231.

ORCID iDs

Jungpyo Lee https://orcid.org/0000-0002-4382-4515

References

[1] Perkins W. 1977 *Nucl. Fusion* **17** 1197
[2] Weynants R.R. 1974 *Phys. Rev. Lett.* **33** 78
[3] Brambilla M. and Ottaviani M. 1985 *Plasma Phys. Control. Fusion* **27** 1
[4] Brambilla M. and Krucken T. 1988 *Plasma Phys. Control. Fusion* **30** 1083
[5] Stix T.H. 1992 *Waves in Plasmas* (New York: Springer)
[6] Porkolab M. 1994 *AIP Conf. Proc.* **314** 99
[7] Lamalle P.U. *et al* 2006 Expanding the operating space of ICRF on JET with a view to ITER *Nucl. Fusion* **46** 391–400
[8] Mayoral M.-L. *et al* 2006 Hydrogen plasmas with ICRF inverted minority and mode conversion heating regimes in the JET tokamak *Nucl. Fusion* **46** S550

[9] Lamalle P.U., Messiaen A.M., Dumortier P. and Louche F. 2006 Recent developments in ICRF antenna modelling *Nucl. Fusion* **46** 432–43
[10] Messiaen A., Dumortier P., Kyrytsya V., Louche F. and Vervier M. 2011 Simulation of ICRF antenna plasma loading by a dielectric dummy load. Application to the ITER case *Fusion Eng. Des.* **86** 855
[11] Durodiea F. *et al* 2009 Commissioning of the ITER-like ICRF antenna for JET *Fusion Eng. Des.* **84** 279
[12] Start D.F.H. *et al* 1999 Nucl. Fusion 39 321 Bulk ion heating with ICRH in JET DT plasmas *Nucl. Fusion* **39** 321
[13] ITER Physics Expert Group on Energetic Particles, Heating and Current Drive and ITER Physics Basis Editors 1999 Chapter 6: Plasma auxiliary heating and current drive *Nucl. Fusion* **39** 2495
[14] Budny R.V. *et al* 2012 *Nucl. Fusion* **52** 023023
[15] Schneider M, Artaud J.-F., Bonoli P., Kazakov Y., Lamalle P., Lerche E., Van Eester D. and Wright J. 2017 *EPJ Web Conf.* **157** 03046
[16] Lee J.P., Smithe D., Jaeger E.F., Harvey R.W. and Bonoli P.T. 2019 *Phys. Plasmas* **26** 012505
[17] Brambilla M. 1999 *Plasma Phys. Control. Fusion* **41** 1
[18] Stix T.H. 1975 *Nucl. Fusion* **15** 737
[19] Jaeger E.F. *et al* 2006 *Nucl. Fusion* **46** S397
[20] Harvey R.W. and McCoy M.G. 1992 The CQL3D Fokker–Planck code *Proc. IAEA Technical Committee Meeting on Advances in Simulation and Modeling of Thermonuclear Plasmas (Montreal, 15 June 1992)* p 489
[21] Kennel C.F. and Engelmann F. 1966 *Phys. Fluids* **9** 2377–88
[22] Jaeger E.F. *et al* 2008 *Phys. Plasmas* **15** 072513
[23] Bilato R., Bertelli N., Brambilla M., Dumont R., Jaeger E.F., Johnson T., Lerche E., Sauter O., Van Eester D. and Villard L. 2015 *AIP Conf. Proc.* **1689** 060001